






Planar Airy beam light-sheet for two-photon microscopy

NEVEEN A. HOSNY,¹  JAMES A. SEYFORTH,¹ GUNNAR SPICKERMANN,¹  THOMAS J. MITCHELL,¹  PEDRO ALMADA,¹ ROBERT CHESTERS,² SCOTT J. MITCHELL,^{2,3} GEORGE CHENNEL,² ANTHONY C. VERNON,^{2,4} KWANGWOOK CHO,^{2,3} DEEPAK P. SRIVASTAVA,^{2,4}  ROBERT FORSTER,¹ AND TOM VETTENBURG^{5,6,*} 

¹*M Squared Life, The Surrey Technology Centre, Guildford, Surrey, GU2 7YG, UK*

²*Basic and Clinical Neuroscience Department, King's College London, London, SE5 9NU, UK*

³*UK Dementia Research Institute, King's College London, London, UK*

⁴*MRC centre For Neurodevelopmental Disorders, King's College London, London, UK*

⁵*School of Physics and Astronomy, University of Exeter, EX4 4QL, Exeter, UK*

⁶*School of Science and Engineering, University of Dundee, DD1 4HN, Dundee, UK*

*t.vettenburg@dundee.ac.uk

Abstract: We demonstrate the first planar Airy light-sheet microscope. Fluorescence light-sheet microscopy has become the method of choice to study large biological samples with cellular or sub-cellular resolution. The propagation-invariant Airy beam enables a ten-fold increase in field-of-view with single-photon excitation; however, the characteristic asymmetry of the light-sheet limits its potential for multi-photon excitation. Here we show how a planar light-sheet can be formed from the curved propagation-invariant Airy beam. The resulting symmetric light sheet excites two-photon fluorescence uniformly across an extended field-of-view without the need for deconvolution. We demonstrate the method for rapid two-photon imaging of large volumes of neuronal tissue.

Published by The Optical Society under the terms of the [Creative Commons Attribution 4.0 License](https://creativecommons.org/licenses/by/4.0/). Further distribution of this work must maintain attribution to the author(s) and the published article's title, journal citation, and DOI.

1. Introduction

Fluorescence light-sheet microscopy has found rapid adoption in developmental biology and the neurosciences [1]. By illuminating a single plane, orthogonal to the detection axis of the microscope, light-sheet microscopy combines high resolution with unparalleled contrast and minimal sample exposure, thus limiting the potential for photo-bleaching and photo-toxic effects [2,3]. However, diffraction limits the field-of-view in which the light-sheet illumination can be confined to a sufficiently thin section. This leads to a loss in contrast and axial resolution in all but the center of the field-of-view, while ineffectively exciting fluorescence elsewhere. Tiling multiple acquisitions [4], or swiping the focus of the light-sheet across the field-of-view may offer reprieve [5,6]. Alternatively, propagation-invariant Bessel and Airy beams can be used to uniformly illuminate the complete field-of-view [7–9]. Light-sheets formed by such beams do have a transversal structure of side-lobes that would lead to poor axial resolution, unless the fluorescence excited by the side lobes is blocked [7], or the main lobe is singled out using structured illumination or two-photon Bessel beam excitation [8].

Single-photon Airy light-sheet illumination can extend the field-of-view by an order of magnitude without requiring any physical filtering of the emitted fluorescence [9,10]. The peculiar asymmetric transversal structure of the illumination enables digital-deconvolution to

reconstruct 3D images with sub-cellular resolution. The image resolution after deconvolution is not determined by the width of the single-photon light-sheet but by the fine-structure of the illumination [9], and the detection point-spread-function [11]. Our aim is to combine the advantages of the Airy beam and two photon excitation in a single device.

Two-photon excitation can double the imaging depth [12–15]; furthermore, the longer wavelengths are less likely to interfere with the photo-receptor cells of the specimen [16]. The ability of the two-photon Bessel beam to excite fluorescence in a thin plane has already been established [7,8]. As an alternative solution, we explore how a planar two-photon Airy light-sheet can be achieved with a minor modification of a single-photon Airy light-sheet microscope. While it has been shown that a two-photon Airy beam light-sheet can extend the field-of-view by a factor of six [17,18], the side-lobes in its transversal structure are suppressed. Although the width of the light-sheet is reduced, the loss in high spatial-frequency components in the two-photon excitation (2PE) profile precludes the digital recovery of the same high axial resolution as seen in its single-photon variant [9]. Notwithstanding, digital deconvolution is essential to correct for the asymmetry of the Airy beam light-sheet and the parabolic trajectory of the Airy beam that forms it [19–21]. Without digital-deconvolution, the asymmetric transversal profile causes imaging artefacts, while the curvature of the light-sheet distorts the three-dimensional image formed by it. Here we show how the Airy beam light-sheet microscope can be modified to produce a uniform plane of illumination that obviates the need for deconvolution.

2. Planar Airy light-sheet

A 2PE light-sheet can be generated by rapidly scanning a femto-second laser beam perpendicular to its propagation direction [22]. When instead of a Gaussian beam, the propagation-invariant Airy beam is used, an extended ‘Airy light-sheet’ is formed [9,17,23]. Although lasers can be designed to directly emit an Airy beam [24], any Gaussian beam can be converted into an Airy beam by introducing a cubic-polynomial phase modulation at a plane conjugate to the back aperture. This can be done using a diffractive spatial light modulator [9], a phase mask, or off-the-shelf cylindrical lenses [10,25]. The phase modulation introduces a position-dependent phase delay $\Delta\phi(u, v) = 2\pi\alpha(u^3 + v^3)$, where u and v are Cartesian coordinates normalized to the radius of the aperture. In our experiments, a phase mask with modulation depth, $\alpha = 10.2$, was found to uniformly illuminate the field-of-view of the 20× detection objective (Section 5.1). For a single-photon Airy beam light-sheet it is advantageous to align the Cartesian axes (u, v) of the phase mask with those of the detection objective (y, z), as shown in the insets of Figs. 1(A,D).

Figure 1(A) shows the transversal profile of a 2PE truncated Gaussian beam (cyan) at $x = 0$, as well as the light-sheet formed by scanning it along the y -axis. As can be seen from the x - z -cross-section of the light-sheet in Fig. 1(B), the truncated Gaussian light-sheet does not illuminate the full width of the field-of-view. Figure 1(D) shows the transversal profile of the 2PE Airy beam (cyan) at $x = 0$ with its Cartesian axes, u and v , parallel to the y and z -axes. The inset in the top-right corner indicates the cubic phase modulation at the back aperture (NA = 0.3). Scanning the beam in the y -direction forms the Airy light-sheet (false-color). The x - z -section in Fig. 1(E) shows the characteristic parabolic trajectory of the Airy beam and the light-sheet it forms throughout the full field-of-view. Although the NA of the truncated Gaussian is only a third (NA = 0.1) of that of the Airy beam, it cannot match its uniformity. Multiple, high-contrast, side-lobes can be observed in the transversal structure parallel to the main intensity lobe of the Airy light-sheet. As can be seen from the comparison with the single-photon excitation (Fig. 1(F)), due to the quadratic scaling of the intensity, the transversal structure is less pronounced for 2PE [9]. Yet, the remaining side-lobes and the curvature of the light-sheet introduce imaging artefacts and distortion. A straightforward modification avoids this, thus eliminating the need for deconvolution and image processing. Figures 1(G,H), show how a planar light-sheet can be formed by rotating the phase modulation 45° around the propagation axis, x , so that the parabolic

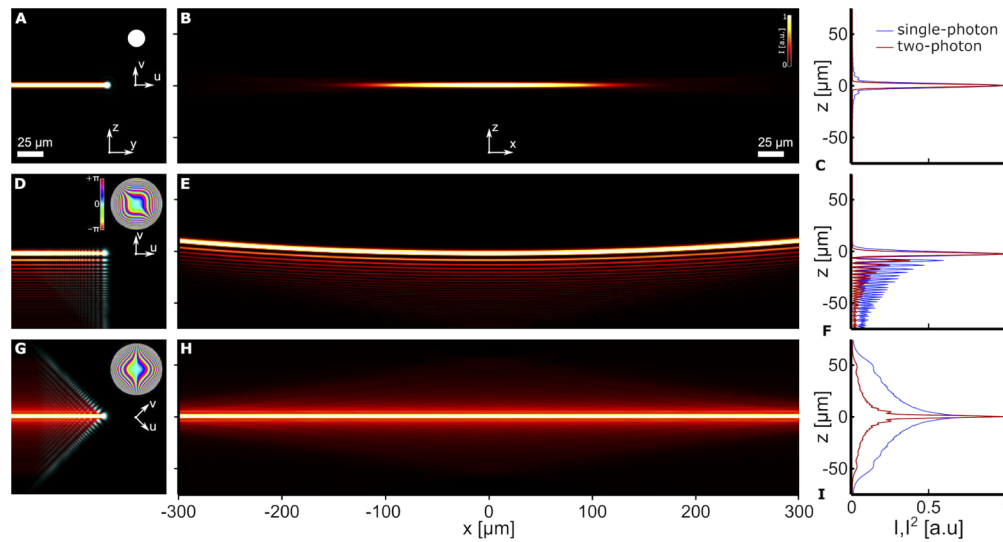


Fig. 1. Depiction of 2PE light-sheet formation by rapidly scanning a truncated Gaussian beam (A-C), an Airy beam with aligned principal axes (D-F), and an Airy beam with its principal axes at 45° to the light-sheet (G-I). The detection objective (not shown) is focused to the x - y -plane and two-photon excited fluorescence is collected along the z -axis. Transversal (y - z) cross-sections are shown in (A,D,G) for the beam waist (magenta) and the 2PE light-sheet (false-color legend in panel (B)). Normalized linear intensity and 2PE for each light-sheet at its waist ($x = 0$) are shown in panels (C,F,I). The inset disks show the relative back aperture size and phase (hue). The numerical apertures (NA) for the Airy beams is 0.30, while that for the truncated Gaussian is chosen to be 0.10 as a larger NA would have resulted in an impractically narrow field-of-view. The extents of the two-photon light-sheets can be seen in panels (B,E,H), which show false-color x - z -sections. (B) It can be seen that even at the lower NA, the truncated Gaussian only illuminates a fraction of the full field-of-view. (E) The Airy beam light-sheet illuminates the full field-of-view; however, the side-lobes of the Airy beam can be seen to form parallel, curved, surfaces. As a result, towards the extremes of the field-of-view, the main lobe does not coincide with the focal plane ($z = 0$). (H) The 45° -rotated Airy beam can be seen to produce a single, planar, excitation surface. (I) By rotating the scanned beam with respect to the light-sheet plane, its side-lobes merge into a single structure (blue), which results in a highly-confined 2PE (red). Most importantly, the excitation coincides with the focal plane throughout the 0.60 mm-wide field-of-view.

trajectory of the Airy beam coincides with the x - y -plane, the focal plane of the detection objective. Furthermore, such planar light-sheet can be seen to have a z -symmetry in its transversal structure, with side-lobes that overlap and blur into a triangular excitation profile (Fig. 1(I)). This negates the need for deconvolution of Airy side lobes and geometric correction of the curved Airy beam. Moreover, since the beam is no longer curved, the depth-of-field of the detection objective is not limited by the illumination, thus enabling the use of high NA detection objectives for optimal lateral resolution.

3. Results and discussion

A 2PE Airy light-sheet was produced by introducing a cubic phase mask in the illumination path of an inverted light-sheet microscope (iSPIM [26]). The cubic phase mask was mounted in a rotation mount to facilitate switching between the conventional (0°) and the planar Airy light-sheet (45°). While the former configuration has been preferred for single photon excitation

and deconvolution [9]; here, we show that the planar Airy light-sheet is highly advantageous when using two-photon excitation.

To quantify its imaging capabilities, a 0.60 mm-wide volume of fluorescent microspheres (ϕ 500 nm) was imaged with 2PE using the conventional Airy light-sheet (Fig. 2(A)) and the planar Airy light-sheet (Fig. 2(B)). Although the NA of the illumination was identically 0.30 in both cases, it is apparent that the illumination of the Airy light-sheet is less uniform than that of the planar Airy light-sheet. To quantify the widths of the field-of-view, the peak intensity of the microspheres was plotted as a function of the absolute distance, $|x|$, from the center of the field-of-view (Fig. 2(E)) for the Airy light-sheet (red) and the planar Airy light-sheet (green). To avoid counting overlapping point-spread functions, only clearly isolated (in 3D) microspheres were considered. A Gaussian curve was fitted to determine the full-width-at-half-maximum (FWHM) of the illuminated field-of-view. The 2PE Airy light-sheet illuminates a field-of-view with a FWHM of approximately $311 \pm 17 \mu\text{m}$, while the planar Airy light-sheet extends this by a third to $415 \pm 11 \mu\text{m}$. The improved uniformity of the illumination also suggests that the planar Airy light-sheet can enable a reduction in laser power and sample exposure.

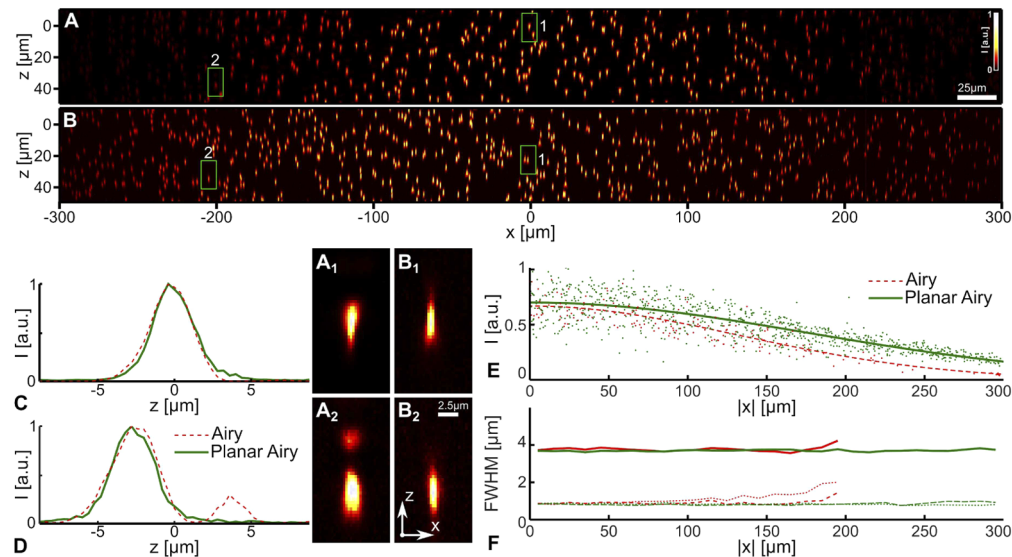


Fig. 2. Comparison of the two-photon Airy beam light-sheet and the two-photon Planar Airy light-sheet for uniformity and resolution. (A,B) Maximum intensity projection of fluorescent microspheres with two-photon fluorescence excited using the conventional Airy light-sheet (A), and the planar Airy light-sheet (B). (C,D) Intensity profiles of four images of isolated fluorescent microspheres near the center of the field-of-view, $x = 0 \mu\text{m}$ (C, A₁, B₁) and near $x = -200 \mu\text{m}$ (D, A₂, B₂); for the conventional Airy light-sheet (red dashed) and the Planar Airy light-sheet (green solid). The locations of the 3D sections are indicated with green rectangles in panels (A) and (B). All false-color images have been normalized to their maximum intensity for clarity. (E) Peak intensity as a function of distance to the field-of-view center $|x|$ for the microspheres illuminated with the conventional Airy light-sheet (red) and the Planar Airy light-sheet (green). To evaluate the illumination uniformity, normal distributions have been fitted to the intensities and found to have a full-width-at-half-maximum field-of-view of $311 \pm 17 \mu\text{m}$ (Airy, dashed red) and $415 \pm 11 \mu\text{m}$ (Planar Airy, green). (F) Full-width at half maximum in x (dashed), y (dotted), and z (solid) of the microsphere images. Median values for every $10 \mu\text{m}$ interval are plotted for microspheres with peak intensities at least 50% above the background.

A closer examination of the images of individual microspheres provides insight into the lack of uniformity of the conventional 2PE Airy light-sheet. Due to the curvature of the conventional Airy light-sheet, its position with respect to the focal plane of the detection objective varies with x in the field-of-view. Figures 2(A₁) and 2(B₁) show microspheres at the center of the field-of-view for the conventional and the planar Airy light-sheet, respectively. The exact location of the sub-volumes is indicated with a green rectangle in Figs. 2(A) and 2(B). Near the center of the field-of-view, the main lobe approximately coincides with the focal plane, resulting in a well-defined image of the microsphere for both the conventional and the planar Airy light-sheet (Figs. 2(A₁), 2(B₁), and 2(C)). Closer to the edge of the field-of-view, two lobes of the transversal structure are distinctly visible in Fig. 2(A₂) for the conventional Airy light-sheet; while the planar Airy light-sheet produces a single, compact, point-spread function (Fig. 2(B₂)). Cross-sections of the microspheres are shown in Fig. 2(D) for comparison. At $|x| \approx 200 \mu\text{m}$, both the main and the second intensity lobe of the transversal profile are within the depth-of-field of the detection objective for the conventional Airy light-sheet, though neither is in optimal focus. In contrast, the planar Airy light-sheet only has a single well-defined plane of high intensity that coincides with the focal plane of the detection objective (Fig. 1(I)). The images of microspheres are therefore relatively independent of the position in the field-of-view, as can be seen by comparing Figs. 2(B₁) and 2(B₂).

As an indication of resolution, the FWHM in the three dimensions and its median are plotted for every 10 μm -interval in Fig. 2(F). The median FWHM in (x, y, z) over the field-of-view are found to be (0.91, 1.02, 3.74) μm for the conventional Airy light-sheet and (0.81, 0.85, 3.69) μm for the Planar Airy light-sheet, respectively. Note that insufficient bright isolated references were detected beyond $|x| \geq 200 \mu\text{m}$ for the conventional Airy light-sheet, while the planar Airy light-sheet ensured that all microspheres near the focal plane were clearly visible. Although these values are an upper bound due to the finite diameter of the microspheres, it is clear that the resolution is relatively constant throughout the field-of-view for the planar Airy light-sheet (Fig. 2(F), green). The lack of side-lobes and curvature of the planar Airy light-sheet simplifies the imaging process and removes several constraints. No deconvolution, nor geometric correction is required with the planar Airy light-sheet. In turn, this obviates Nyquist sampling in the axial dimension ($\Delta z = 0.4 \mu\text{m}$), thereby enabling faster volumetric recording. The numerical aperture of the detection objective can be chosen so that its Rayleigh range matches the planar Airy light-sheet's transverse profile.

Figure 3 shows neurons from organotypic cultured hippocampal slices of male Wistar rat. The neurons express the fluorescent protein mVenus (see Methods Section 5.2.2). Two-photon planar Airy light-sheet imaging enables the rapid visualization of synaptic function and microstructure with high resolution in live tissue, thus facilitating investigations into the relationship between neuronal structure and function. The neurons extend over the $x \times y \times z = 0.60 \times 0.60 \times 0.50 \text{ mm}^3$ imaging volume. Panels (A) and (B) show projections along the y and x -axis, respectively. It can be noted that the two-photon excitation yields uniform image quality throughout the 0.60 mm-wide imaging volume. High-resolution features are clearly visible, including sub-micron dendritic spines. Panels (C) displays the zoomed-in volume around a single neuron, showing its dendritic tree, while panel (D) shows a 5 \times further enlarged sub-volume around a single dendrite. Examples of dendritic spines are indicated by white arrow heads.

Larger volumes can be imaged by increasing the scan distance along the z -axis or by tiling multiple acquisition volumes in the x or y -direction. The latter is demonstrated by acquiring neighboring $0.60 \times 0.60 \times 0.60 \text{ mm}^3$ volumes of cleared mouse brain tissue. Two side-by-side stacks were acquired to produce a $y = 1.15 \text{ mm}$ -tall 3D data cube. Maximum intensity projections are shown in Fig. 4. Each stack consists of 500 slices, with a slice-spacing of 1.2 μm , and illuminated with the planar Airy light-sheet for a duration of 50 ms. This resulted in an

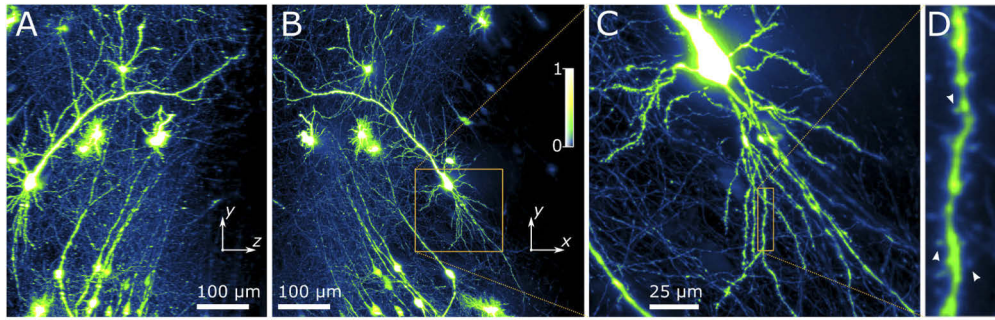


Fig. 3. Maximum intensity projection of $0.60 \times 0.60 \times 0.60 \text{ mm}^3$ of Wistar rat hippocampal tissue, imaged using the two-photon planar Airy light-sheet. (A) The z - y -projection along the x -axis of the volume indicated by the yellow dash-dotted box in panel (B). The variation in axial (z) resolution can be seen to be minimal. (B) The x - y -projection along the z -axis, showing high lateral resolution throughout the $0.6 \times 0.6 \times 0.5 \text{ mm}^3$ field-of-view. (C) Magnified 3D slice of the data cube, indicated by the orange rectangle in panel (B). (D) A further 5 \times enlargement of the magnified sub-volume indicated by the orange rectangle in panel (C). White arrowheads indicate examples of dendritic spines.

acquisition time of 25 s/stack. A three-dimensional view from a rotating perspective can be seen in accompanying [Visualization 1](#).

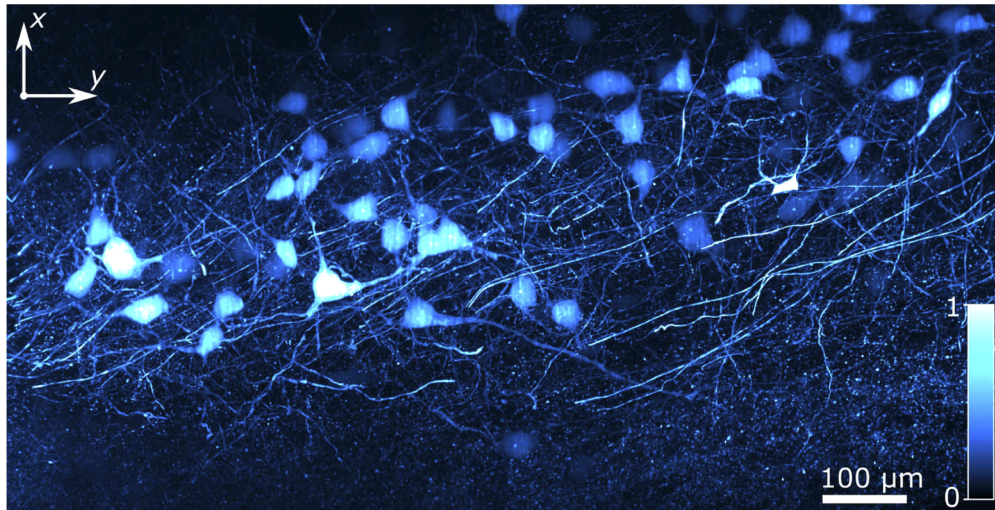


Fig. 4. Maximum intensity projection of $x \times y \times z = 0.60 \times 1.15 \times 0.60 \text{ mm}^3$ of Thy-1-GFP-expressing mouse brain tissue, imaged using the two-photon planar Airy light-sheet. A video showing additional viewpoints is included as [Visualization 1](#).

4. Conclusion

We have demonstrated how a planar Airy light-sheet can be realized based on the propagation-invariant, yet curved, Airy beam. The symmetric intensity profile of the planar Airy light-sheet eliminates any requirement for deconvolution and image processing. We characterized the performance of the planar Airy light-sheet microscope and demonstrate how it can be effective for

rapid imaging of large volumes of neuronal tissue with two-photon excitation. The propagation-invariant Airy beam can potentially be generated by combining low-cost off-the-shelf cylindrical lenses [27]. We anticipate that the advantages of this method will be further enhanced with higher-order non-linearities to image deeper into tissue [28].

5. Methods

5.1. Optical set-up and image formation

An Airy beam light-sheet microscope in iSPIM configuration [9,22,26] is modified to enable the axial rotation of the beam shaping optics. A cubic phase modulation introduces a phase delay, $\Delta\phi(u, v) = 2\pi\alpha(u^3 + v^3)$, in the illumination beam before reimaging it to the back aperture of the illumination objective (Olympus 10× NA 0.30). Here, u and v are Cartesian coordinates, centered at the back-aperture and normalized to its radius, while α is a unit-less constant that is approximately proportional to the propagation invariance of the light-sheet [9]. The value of α was determined to be 10.2 at a wavelength of 930.9 nm for 2PE. To enable switching between a conventional Airy light-sheet and a planar Airy light-sheet, the phase modulation can be rotated by 45° around the optical axis. Fluorescence emission is collected using a second water dipping objective (Olympus 20× NA 0.50), orthogonal to the excitation plane, and refocused onto the sensor array (Orca Flash 4.0 v2). Using a galvanometer mirror, the Airy beam is scanned along the y -axis during the acquisition of each single-plane image. A three-dimensional volume is acquired by motorized translation of the sample orthogonally to the focal plane.

Two-photon excitation was achieved using a mode-locked Ti:Sapphire mode-locked laser (Sprite XT, M Squared Lasers, UK), at a wavelength of $\lambda = 930.9$ nm, a pulse duration of 140 fs and a repetition rate of 80 MHz.

No geometric correction or image deconvolution is used. Raw data is analyzed and visualized using Matlab (MathWorks, USA) and FIJI [29]. Imaris Image Analysis Software (Oxford Instruments, UK) was used to create a three-dimensional visualization.

5.2. Sample preparation

5.2.1. Fluorescent microspheres

To experimentally verify the resolution and uniformity, image stacks of a phantom sample were acquired. Fluorescent microspheres (ϕ 500 nm Tetraspeck, Thermofisher UK) were sparsely suspended in low melting point 1.2% agarose (Ultrapure, Invitrogen), loaded in to a sample chamber and immersed in water. Using the beads allowed the resolution and brightness to be evaluated as a function of the position in the field-of-view.

5.2.2. Biological samples

All procedures were carried out in accordance with the UK Animals (Scientific Procedures) Act, 1986. All animal experiments were given ethical approval by the ethics committee of King's College London (UK).

The biological samples used in the experiments were held in place with a thin layer of low melting point 1.2% agarose on Polydimethylsiloxane (PDMS) plinths inside the samples chambers.

Mouse brain tissue. Brain tissue from adult male mice expressing Thy-1-GFP (Tg(Thy1-EGFP)MJrs/J; a generous gift from Professor Robert Hindges, King's College London) was fixed and rendered optically transparent using passive CLARITY [30].

Organotypic hippocampal slice culture and transfection. Male 7-day old Wistar rats (Charles River, UK) were used to prepare organotypic hippocampal slices for live imaging. The organotypic hippocampal slice culture (Fig. 3) was prepared as previously described [31]. All steps were carried out under sterile conditions. Briefly, schedule 1 procedure was performed,

rat brains rapidly removed and placed into ice-cold dissecting medium containing: 238 mM sucrose, 2.5 mM KCl, 26 mM NaHCO₃, 1 mM NaH₂PO₄, 5 mM MgCl₂, 11 mM D-glucose and 1 mM CaCl₂. Hippocampi were removed and transverse hippocampal slices (350 μ m) were cut. Following washing, slices were placed upon sterile, semi-porous membranes (Millipore, USA) and stored at the interface between air and culture medium containing: 78.8% minimum essential medium with L-glutamine, 20% heat-inactivated horse serum, 30 mM HEPES, 26 mM D-glucose, 5.8 mM NaHCO₃, 2 mM CaCl₂, 2 mM MgSO₄, 70 μ M ascorbic acid and 1 μ g mL⁻¹ insulin (pH adjusted to 7.3 and 320 – 330 mOsm kg⁻¹). The slices were then cultured in an incubator (35 °C, 5% CO₂) for 7 – 10 days in vitro (DIV). The medium was changed every 2 days. Neurons were transfected with mVenus using a biolistic gene gun (Helios Gene-gun system, Bio Rad, U.S.A.) at DIV 4. Imaging assays were performed 5 days after transfection (DAT) [32]. The mVenus fluorescent protein was expressed throughout the cells to allow visualization of the neuronal architecture.

Funding

Open Innovation Funding Platform Award (University of Exeter) (PS-CEMPS-4786); UK Research and Innovation (Future Leaders Fellowship, MR/S034900/1); Royal Society (RG130610).

Acknowledgments

We would like to thank Professor Robert Hindges, King's College London, for the generous gift of the Thy1-GFP expressing mice; as well as the Wohl Cellular Imaging Centre for their help with this study. This research project was supported by Open Innovation Funding Platform Award (University of Exeter) and M Squared Life Ltd (PS-CEMPS-4786). A.C.V. acknowledges financial support from the Royal Society that contributed to this work (Research Grant, RG130610); S.J.M and K.C were funded by the UK Dementia Research Institute which receives its funding from DRI Ltd, funded by the UK Medical Research Council, Alzheimer's Society and Alzheimer's Research UK (grant number UK-DRI RE13559). This work was supported by a UKRI Future Leaders Fellowship grant, number MR/S034900/1.

Disclosures

NAH, JAS, GS, TJM, PA, RF: M Squared Life (E,P), TV: University of Dundee (F,P)

References

1. E. M. Hillman, V. Voleti, W. Li, and H. Yu, "Light-sheet microscopy in neuroscience," *Annu. Rev. Neurosci.* **42**(1), 295–313 (2019). PMID: 31283896.
2. J. Huysken, J. Swoger, F. D. Bene, J. Wittbrodt, and E. H. K. Stelzer, "Optical sectioning deep inside live embryos by selective plane illumination microscopy," *Science* **305**(5686), 1007–1009 (2004).
3. M. B. Ahrens, M. B. Orger, D. N. Robson, J. M. Li, and P. J. Keller, "Whole-brain functional imaging at cellular resolution using light-sheet microscopy," *Nat. Methods* **10**(5), 413–420 (2013).
4. Q. Fu, B. L. Martin, D. Q. Matus, and L. Gao, "Imaging multicellular specimens with real-time optimized tiling light-sheet selective plane illumination microscopy," *Nat. Commun.* **7**(1), 11088 (2016).
5. K. M. Dean, P. Roudot, E. S. Welf, G. Danuser, and R. Fiolka, "Deconvolution-free subcellular imaging with axially swept light sheet microscopy," *Biophys. J.* **108**(12), 2807–2815 (2015).
6. T. Chakraborty, M. K. Driscoll, E. Jeffery, M. M. Murphy, P. Roudot, B.-J. Chang, S. Vora, W. M. Wong, C. D. Nielson, H. Zhang, V. Zhemkov, C. Hiremath, E. D. De La Cruz, Y. Yi, I. Bezprozvanny, H. Zhao, R. Tomer, R. Heintzmann, J. P. Meeks, D. K. Marciano, S. J. Morrison, G. Danuser, K. M. Dean, and R. Fiolka, "Light-sheet microscopy of cleared tissues with isotropic, subcellular resolution," *Nat. Methods* **16**(11), 1109–1113 (2019).
7. F. O. Fahrbach, P. Simon, and A. Rohrbach, "Microscopy with self-reconstructing beams," *Nat. Photonics* **4**(11), 780–785 (2010).
8. T. A. Planchon, L. Gao, D. E. Milkie, M. W. Davidson, J. A. Galbraith, C. G. Galbraith, and E. Betzig, "Rapid three-dimensional isotropic imaging of living cells using Bessel beam plane illumination," *Nat. Methods* **8**(5), 417–423 (2011).

9. T. Vettenburg, H. I. C. Dalgarno, J. Nylk, C. C. Lladó, D. E. K. Ferrier, T. Čížmár, F. J. Gunn-Moore, and K. Dholakia, "Light sheet microscopy using an Airy beam," *Nat. Methods* **11**(5), 541–544 (2014).
10. Z. Yang, M. Prokopas, J. Nylk, C. Coll-Lladó, F. J. Gunn-Moore, D. E. K. Ferrier, T. Vettenburg, and K. Dholakia, "A compact Airy beam light sheet microscope with a tilted cylindrical lens," *Biomed. Opt. Express* **5**(10), 3434–3442 (2014).
11. O. E. Olarte, J. Andilla, D. Artigas, and P. Loza-Alvarez, "Decoupled illumination detection in light sheet microscopy for fast volumetric imaging," *Optica* **2**(8), 702–705 (2015).
12. T. V. Truong, W. Supatto, D. S. Koos, J. M. Choi, and S. E. Fraser, "Deep and fast live imaging with two-photon scanned light-sheet microscopy," *Nat. Methods* **8**(9), 757–760 (2011).
13. O. E. Olarte, J. Licea-Rodriguez, J. A. Palero, E. J. Gualda, D. Artigas, J. Mayer, J. Swoger, J. Sharpe, I. Rocha-Mendoza, R. Rangel-Rojo, and P. Loza-Alvarez, "Image formation by linear and nonlinear digital scanned light-sheet fluorescence microscopy with Gaussian and Bessel beam profiles," *Biomed. Opt. Express* **3**(7), 1492–1505 (2012).
14. Z. Lavagnino, F. C. Zanicchi, E. Ronzitti, and A. Diaspro, "Two-photon excitation selective plane illumination microscopy (2PE-SPIM) of highly scattering samples: characterization and application," *Opt. Express* **21**(5), 5998–6008 (2013).
15. W. Zong, J. Zhao, X. Chen, Y. Lin, H. Ren, Y. Zhang, M. Fan, Z. Zhou, H. Cheng, Y. Sun, and L. Chen, "Large-field high-resolution two-photon digital scanned light-sheet microscopy," *Cell Res.* **25**(2), 254–257 (2015).
16. S. Wolf, W. Supatto, G. Debregeas, P. Mahou, S. G. Kruglik, J.-M. Sintes, E. Beaurepaire, and R. Candelier, "Whole-brain functional imaging with two-photon light-sheet microscopy," *Nat. Methods* **12**(5), 379–380 (2015).
17. P. Piksarv, D. Marti, T. Le, A. Unterhuber, L. H. Forbes, M. R. Andrews, A. Stingl, W. Drexler, P. E. Andersen, and K. Dholakia, "Integrated single-and two-photon light sheet microscopy using accelerating beams," *Sci. Rep.* **7**(1), 1435 (2017).
18. X.-J. Tan, C. Kong, Y.-X. Ren, C. S. W. Lai, K. K. Tsia, and K. K. Y. Wong, "Volumetric two-photon microscopy with a non-diffracting Airy beam," *Opt. Lett.* **44**(2), 391–394 (2019).
19. G. A. Siviloglou and D. N. Christodoulides, "Accelerating finite energy Airy beams," *Opt. Lett.* **32**(8), 979–981 (2007).
20. G. A. Siviloglou, J. Broky, A. Dogariu, and D. N. Christodoulides, "Observation of accelerating Airy beams," *Phys. Rev. Lett.* **99**(21), 213901 (2007).
21. A. D. Jeffrey, J. M. Mark, M. A. Bandres, and D. M. Cottrell, "Observation of accelerating parabolic beams," *Opt. Express* **16**(17), 12866–12871 (2008).
22. P. J. Keller and E. H. K. Stelzer, "Quantitative in vivo imaging of entire embryos with digital scanned laser light sheet fluorescence microscopy," *Curr. Opin. Neurobiol.* **18**(6), 624–632 (2008).
23. M. V. Berry and N. L. Balazs, "Nonspread wave packets," *Am. J. Phys.* **47**(3), 264–267 (1979).
24. G. Porat, I. Dolev, O. Barlev, and A. Arie, "Airy beam laser," *Opt. Lett.* **36**(20), 4119–4121 (2011).
25. J. Wang, J. Bu, M. Wang, Y. Yang, and X. Yuan, "Generation of high quality airy beams with blazed micro-optical cubic phase plates," *Appl. Opt.* **50**(36), 6627–6631 (2011).
26. Y. Wu, A. Ghitani, R. Christensen, A. Santella, Z. Du, G. Rondeau, Z. Bao, D. Colón-Ramos, and H. Shroff, "Inverted selective plane illumination microscopy (ispim) enables coupled cell identity lineaging and neurodevelopmental imaging in *Caenorhabditis elegans*," *Proc. Natl. Acad. Sci. U. S. A.* **108**(43), 17708–17713 (2011).
27. D. G. Papazoglou, S. Suntsov, D. Abdollahpour, and S. Tzortzakis, "Tunable intense Airy beams and tailored femtosecond laser filaments," *Phys. Rev. A* **81**(6), 061807 (2010).
28. A. Escobet-Montalbán, F. M. Gasparoli, J. Nylk, P. Liu, Z. Yang, and K. Dholakia, "Three-photon light-sheet fluorescence microscopy," *Opt. Lett.* **43**(21), 5484–5487 (2018).
29. J. Schindelin, I. Arganda-Carreras, E. Frise, V. Kaynig, M. Longair, T. Pietzsch, S. Preibisch, C. Rueden, S. Saalfeld, B. Schmid, J.-Y. Tinevez, D. J. White, V. Hartenstein, K. Eliceiri, P. Tomancak, and A. Cardona, "Fiji: an open-source platform for biological-image analysis," *Nat. Methods* **9**(7), 676–682 (2012).
30. R. Tomer, L. Ye, B. Hsueh, and K. Deisseroth, "Advanced clarity for rapid and high-resolution imaging of intact tissues," *Nat. Protoc.* **9**(7), 1682–1697 (2014).
31. J. H. Yi, D. H. Kim, T. M. Piers, S. C. Kim, D. J. Whitcomb, P. Regan, and K. Cho, "Postsynaptic p47phox regulates long-term depression in the hippocampus," *Cell Discovery* **4**(1), 44 (2018).
32. J. H. Yi, C. Brown, G. Whitehead, T. Piers, Y. S. Lee, C. Martinez Perez, P. Regan, D. J. Whitcomb, and K. Cho, "Glucocorticoids activate a synapse weakening pathway culminating in tau phosphorylation in the hippocampus," *Pharmacol. Res.* **121**, 42–51 (2017).